Journal of ELECTRONIC MATERIALS, Vol. 49, No. 3, 2020
https://doi.org/10.1007/s11664-019-07927-8

A Physics-Based Compact Static and Dynamic Characteristics Model for $Al_2O_3/In_xAl_{1-x}N$/AlN/GaN MOS-HEMTs

ABBES BELOUFA,[1,2,4,5] DRISS BOUGUENNA,[1,6,7] NAWEL KERMAS,[1] and DONAT JOSEF AS[3,8]

1.—Laboratory of Geomatics, Ecology and Environment (LGEO2E), Department of Science and Technology, University Mustapha Stambouli of Mascara, 29000 Mascara, Algeria. 2.—Applied Materials Laboratory, University of Sidi Bel Abbès, 22000 Sidi Bel Abbès, Algeria. 3.—Department of Physics, University of Paderborn, 33098 Paderborn, Germany. 4.—e-mail: beloufa.abbes@univ-mascara.dz. 5.—e-mail: a_beloufa@yahoo.fr. 6.—e-mail: dbouguenna29@gmail.com. 7.—e-mail: bouguenna.driss@univ-mascara.dz. 8.—e-mail: d.as@unipaderborn.de

This paper presents a physics-based compact of indium mole fraction dependent analytical model for static and dynamic characteristics of GaN-based MOS-HEMTs. The model covers all the different operating regimes of the MOS-HEMT devices. The model is evaluated step by step with excellent agreement compared with the simulated data obtained by Atlas-TCAD simulation and the experimental data have demonstrated the validity of the proposed model for different indium mole fractions (12, 15, 17, and 18)%. From static and dynamic characteristics, it is also observed that by careful setting of the indium mole fraction for GaN-based MOS-HEMTs can improve the performance of the device, and; hence, it is proper for high performance low loss applications. MOS-HEMTs produce high drain current of 1227 A/m at a positive gate bias V_{gs} of 3 V and with 15% of indium mole fraction, high transconductance of 268 S/m, and high cut-off frequency of 35 GHz at x = 18% indium mole fraction.

Key words: $Al_2O_3/In_xAl_{1-x}N$/AlN/GaN, MOS-HEMTs, indium mole fraction, Atlas-TCAD

INTRODUCTION

Over the past several years, the scientific research on the properties of $In_xAl_{1-x}N$ material system was only scarce data intensified since 2005.[1] In fact, the AlGaN/GaN heterostructures material system was well-established for high power and high frequency electronic devices.[2] Recently, $In_xAl_{1-x}N$ material system as a new barrier layer has been implemented instead of AlGaN and, as an alternative lattice-matched for nitride-based high electron mobility transistors (HEMTs), was proposed by Kuzmik[3] to improve the HEMTs performance.

Newly, $In_xAl_{1-x}N$/GaN HEMTs have attracted more attention due to their demonstrated superior thermal stability and high current density.[3] Indeed, one of the main features of the lattice-matched $In_xAl_{1-x}N$/GaN heterostuctures is the possibility to keep a high polarization induced sheet charge density at the heterointerface even for a vanishing piezoelectric component due to the absence of strain.[4]

Therefore, $In_xAl_{1-x}N$/GaN MOS-HEMTs can be of superior performance in comparison to more conventional AlGaN/GaN MOS-HEMTs mostly due to the substantially higher polarization induced two dimensional electron gas density (2-DEG).[5] The insertion of a thin AlN interlayer spacer between the $In_xAl_{1-x}N$ barrier and buffer layers helps to reduce the remote ionized impurity and achieve high 2-DEG mobility in InAlN/GaN heterostuctures, and it can be realized as well.[6] The optimum

(Received September 22, 2019; accepted December 24, 2019; published online January 2, 2020)

AlN interlayer spacer thickness around 1 nm is required for high electron mobility.[7] The electrical properties such as surface of the material, gate leakage, trap densities in the bulk and large dispersion of the transconductance of $In_xAl_{1-x}N/AlN/GaN$ MOS-HEMTs are still some obstacles in the literature of this article's scope.

In this paper, we report on analytical models for the static and dynamic characteristics of GaN-based MOS-HEMTs with Al_2O_3 oxide gate insulation. An analysis of the unified charge density for all regimes of the device operation is a primary requirement for the development of a physics-based compact model for these devices.[8] Recently, Jena et al.[9,10] presented their work on a threshold voltage, 2-DEG density, drain current, total charge, tranconductance and gate-source/gate-drain capacitances GaN-based MOS-HEMTs based on the device physics. However, the effect of the indium mole fraction is not considered in their work.

The rest of the paper is organized as follows. "MOS-HEMTs Structure and Energy Band Diagram" section describes the target of $Al_2O_3/In_xAl_{1-x}N/AlN/GaN$ MOS-HEMT devices structure. In "Analytical Model of the Electrical Properties and Performances" section we derive expressions of the indium mole fraction dependences in the threshold voltage, the drain current, the transconductance, the capacitances, and the cut-off frequency model presented. In "Results and Discussion" section, model results are presented and discussed by comparing them with necessary numerical simulation results obtained from MATLAB and Atlas-TCAD. The experimental data have demonstrated the validity of the proposed model. The paper is finally concluded in "Conclusion" section.

MOS-HEMTS STRUCTURE AND ENERGY BAND DIAGRAM

The cross-sectional view of $In_xAl_{1-x}N/AlN/GaN$ MOS-HEMTs is shown in Fig. 1 presented in this paper. The layer sequence is from top to bottom, metal/Al_2O_3/*n*-$In_xAl_{1-x}N$/undoped-AlN/undoped-GaN with a 2-DEG formed at the unintentionally doped (UIN)-AlN/GaN interface. GaN buffer layer is employed on SiC substrate.[9,10] The device is simulated using a commercially available Atlas-TCAD simulator,[11] to understand the device characteristics of the proposed $Al_2O_3/In_xAl_{1-x}N/AlN/GaN$ MOS-HEMTs. A thin oxide is inserted between Schottky contact and AlInN barrier layer to reduce gate leakage current.[10] Figure 2 shows the conduction energy band diagram of $Al_2O_3/In_xAl_{1-x}N/AlN/GaN$ heterostucture.[9]

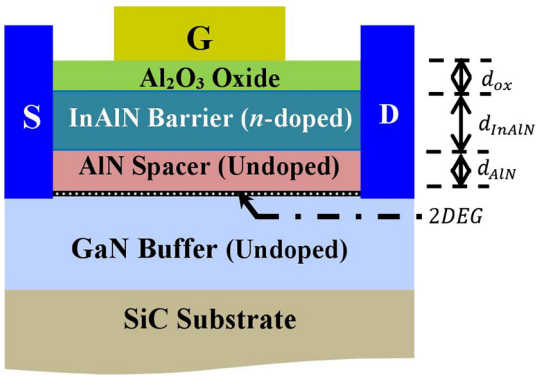

Fig. 1. Cross-sectional view of $Al_2O_3/In_xAl_{1-x}N/AlN/GaN$ MOS-HEMTs with L_g, d_{ox}, d_{InAlN}, and d_{AlN} represent gate length, Al_2O_3 oxide layer thickness, *n*-$In_xAl_{1-x}N$ barrier layer thickness, and AlN spacer layer thickness, respectively.

ANALYTICAL MODEL OF THE ELECTRICAL PROPERTIES AND PERFORMANCES

Threshold Voltage Model for $In_xAl_{1-x}N/AlN/GaN$ MOS-HEMTs

The amount of indium mole fraction (x) available in the barrier layer of $In_xAl_{1-x}N$ greatly influences the device behavior. The Schottky barrier height φ_{eff}, the dielectric constant of the barrier layer ε, the conduction band offset, the total polarization σ_{total}, and the threshold voltage are among the important parameters that are affected by the indium mole fraction.

The balance equation can be set up going from the left to the right according to the energy band diagram of the $Al_2O_3/In_xAl_{1-x}N/AlN/GaN$ MOS-HEMTs as shown in the Fig. 2 respecting the AlN interlayer. Then the balance equation can be written as follows[9]

$$q\varphi_{eff}(x) - \left(\frac{qQ_f}{C_{ox}}\right) - qE_C^{In_xAl_{1-x}N} \times d_{In_xAl_{1-x}N} + \Delta E_C^{In_xAl_{1-x}N/AlN} - qE_C^{AlN} \times d_{AlN} - \Delta E_C^{AlN/GaN}(x) + E_0 + (E_F - E_0) = 0. \quad (1)$$

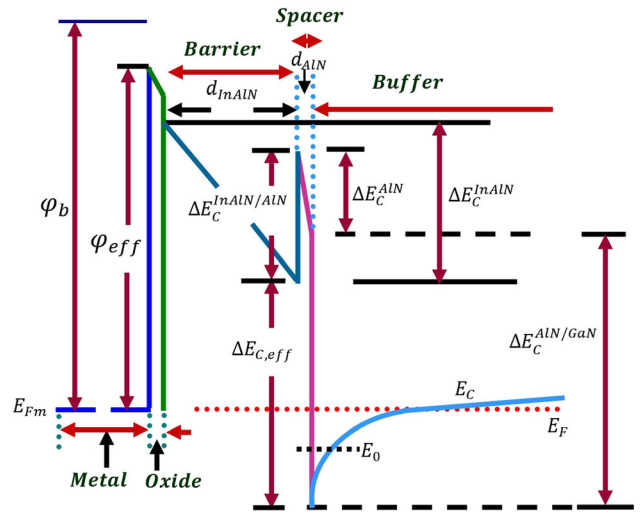

Fig. 2. Conduction energy band diagram of $Al_2O_3/In_xAl_{1-x}N/AlN/GaN$ metal–oxide–semiconductor high electron mobility transistors MOS-HEMTs.

where $\varphi_{\text{eff}}(x)$ is the effective Schottky barrier height of the gate contact and in the case of $In_xAl_{1-x}N$ barrier layer can be expressed using the Vegard's interpolation formula[12]

$$\varphi_{\text{eff}}(x) = 3.05 - 3.7x. \tag{2}$$

$Q_f = E_C^{\text{ox}} \times \varepsilon_0\varepsilon_{\text{ox}} - (\sigma_{\text{ox}/In_xAl_{1-x}N} + \sigma_{In_xAl_{1-x}N/AlN} + \sigma_{AlN/GaN} - n_s)$ is the equivalent charge at the $Al_2O_3/In_xAl_{1-x}N$ interface and E_C^{ox} represents electric field across the dielectric layer.

$E_C^{\text{ox}} = (Q_f + \sigma_{\text{ox}/In_xAl_{1-x}N} + \sigma_{In_xAl_{1-x}N/AlN} + \sigma_{AlN/GaN}/\varepsilon_0\varepsilon_{\text{ox}})$ is the electric field across.

$E_C^{In_xAl_{1-x}N} = [(\sigma_{In_xAl_{1-x}N/AlN} + \sigma_{AlN/GaN})/\varepsilon_0\varepsilon_{In_xAl_{1-x}N}]$ is the electric field across.

The total induced net polarization density (σ_{total}) is the sum of spontaneous and piezoelectric polarizations P_{sp} and P_{pz}, respectively, which forms at the heterointerface, can be defined by Ref. 8

$$\begin{aligned}\sigma_{\text{total}} &= P_{\text{sp}} + P_{\text{pz}} \\ &= \left(P^{\text{GaN}} + P^{\text{AlN}}\right) - \left(P^{\text{AlN}} + P^{In_xAl_{1-x}N}\right) \\ &= P^{\text{GaN}} - P^{In_xAl_{1-x}N} \\ &= P_{\text{sp}}^{\text{GaN}} - \left(P_{\text{sp}}^{In_xAl_{1-x}N} + P_{\text{pz}}^{In_xAl_{1-x}N}\right).\end{aligned} \tag{3}$$

The net polarization charge at the $In_xAl_{1-x}N/AlN$ heterointerface expressed as

$$\begin{aligned}\sigma_{In_xAl_{1-x}N/AlN} = &\left(P_{\text{sp}}^{\text{AlN}} + P_{\text{pz}}^{\text{AlN}}\right) \\ &- \left(P_{\text{sp}}^{In_xAl_{1-x}N} + P_{\text{pz}}^{In_xAl_{1-x}N}\right).\end{aligned} \tag{4}$$

where the piezoelectric polarization of undoped GaN can be neglected for 2 μm layer thickness and only the spontaneous polarization is involved. A nonlinear spontaneous polarization for $In_xAl_{1-x}N$ nitride alloy, in (C/m^2), can be expressed as[13,14]

$$P_{\text{sp}}^{In_xAl_{1-x}N} = -0.042x - 0.090(1-x) + 0.071x(1-x). \tag{5}$$

The piezoelectric polarization of the barrier layer $P_{\text{pz}}^{In_xAl_{1-x}N}$ is considerable, which means that is not strain free, it can be expressed as[15]

$$P_{\text{pz}}^{In_xAl_{1-x}N} = \left[xP_{\text{pz}}^{\text{InN}} + (1-x)P_{\text{pz}}^{\text{AlN}}\right]\epsilon(x), \tag{6}$$

with $P_{\text{pz}}^{In_xAl_{1-x}N}$, $P_{\text{pz}}^{\text{InN}}$ and $P_{\text{pz}}^{\text{AlN}}$ are the piezoelectric polarizations of $In_xAl_{1-x}N$, InN and AlN, respectively.

The piezoelectric polarizations of the relevant binary compounds InN and AlN, in (C/m^2), can be expressed as

$$P_{\text{pz}}^{\text{InN}} = [7.559\epsilon(x) - 1.373]\epsilon(x), \tag{6a}$$

$$P_{\text{pz}}^{\text{AlN}} = [5.624\epsilon(x) - 1.808]\epsilon(x), \tag{6b}$$

where $\epsilon(x)$ is the basal strain field of the ternary compound and an equilibrium lattice constant $a_{In_xAl_{1-x}N}$ as a function of the in-plane strain of the $In_xAl_{1-x}N$ layer, is defined as follows

$$\epsilon(x) = \frac{\left(a_{\text{AlN}} - a_{In_xAl_{1-x}N}\right)}{a_{In_xAl_{1-x}N}}, \tag{6c}$$

where $a_{In_xAl_{1-x}N}$ and a_{AlN} corresponding to the lattice constants of the unstrained and strained $In_xAl_{1-x}N$, respectively. With the in-plane strain in the barrier layer of the $In_xAl_{1-x}N/AlN/GaN$ MOS-HEMTs.[16]

The lattice parameter of unstrained $a_{In_xAl_{1-x}N}$ was derived by applying Vegard's interpolation and is given by Eq. 7[12]

$$a_{In_xAl_{1-x}N} = xa_{\text{InN}} + (1-x)a_{\text{AlN}}. \tag{7}$$

The dielectric constant for the $In_xAl_{1-x}N$ and AlN can be determined from the approximation as follows,[5] the dielectric constant as a function of indium mole fraction for $In_xAl_{1-x}N$ alloy is obtained by

$$\varepsilon_{In_xAl_{1-x}N} = 4.12x + 2.78. \tag{8}$$

E_C^{AlN} is the electrical field across the AlN interlayer and can be approximated by Ref. 9

$$E_C^{\text{AlN}} = \frac{\sigma_{\text{AlN/GaN}}}{\varepsilon_0\varepsilon_{\text{AlN}}}. \tag{9}$$

with $\sigma_{\text{AlN/GaN}}$ is the total polarization, n_s is the charge density across an AlN/GaN interface and d_{AlN} is the AlN interlayer thickness.

$\Delta E_C^{\text{AlN/GaN}}$ and $\Delta E_C^{In_xAl_{1-x}N/AlN}$ are the band offsets between the interface of AlN/GaN and $In_xAl_{1-x}N/AlN$, respectively.

Also, the conduction band offset at the $In_xAl_{1-x}N/AlN$ heterointerface is given by

$$\Delta E_C^{In_xAl_{1-x}N/AlN} = 0.63\left[E_g^{In_xAl_{1-x}N} - E_g^{\text{AlN}}\right], \tag{10}$$

where $E_g^{In_xAl_{1-x}N}$ is the energy band gap of $In_xAl_{1-x}N$ layer as a function of indium mole fraction, and is given by Ref. 17

$$E_g^{In_xAl_{1-x}N} = E_g^{\text{InN}}x + E_g^{\text{AlN}}(1-x) - bx(1-x), \tag{11}$$

with $E_g^{\text{InN}} = 0.95\,\text{eV}$, $E_g^{\text{AlN}} = 6.06\,\text{eV}$ and $b = 3.4x + 1.2$ is the band gap bowing parameter.[7]

In our calculations the doping density of barrier $In_xAl_{1-x}N$ layer is assumed as $N_d = 10^{25}\,\text{m}^{-3}$.

The expression of threshold voltage is derived that depends on the parameters influenced by the mole fraction (x), in order to make this device completely cut-off, it is required to make the 2-DEG

system devoid of electrons and for which external potential has to be applied from the gate terminal. Assuming $n_s = 0\,\mathrm{cm}^{-2}$ in the Eq. 1 and solving for threshold voltage, is given by

$$V_{\mathrm{th}} = q\left[\varphi_{\mathrm{eff}}(x) - E_C^{\mathrm{ox}} \times d_{\mathrm{ox}} - E_C^{\mathrm{In_xAl_{1-x}N}} \times d_{\mathrm{In_xAl_{1-x}N}} - E_C^{\mathrm{AlN}} \times d_{\mathrm{AlN}}\right] - \Delta E_C^{\mathrm{ox/In_xAl_{1-x}N}} + \Delta E_C^{\mathrm{In_xAl_{1-x}N/AlN}} - \Delta E_C^{\mathrm{AlN/GaN}}. \tag{12}$$

Two-DEG Sheet Carrier Density Control Model

The expression for 2-DEG sheet carrier density is a calculated region rise as in Ref. 9 and can be expressed as

$$n_s = \frac{\varepsilon(x)}{qd_T}\left(V_{\mathrm{g0}} - E_{\mathrm{F}}\right), \tag{13}$$

where q represents electronic charge, $\varepsilon(x) = \varepsilon_0\left(\varepsilon_{\mathrm{In_xAl_{1-x}N}} + \varepsilon_{\mathrm{AlN}}\right)$ is the total permittivity, ε_0 is the vacuum permittivity. $\varepsilon_{\mathrm{In_xAl_{1-x}N}}$ and $\varepsilon_{\mathrm{AlN}}$ are the electrical permittivity of $In_xAl_{1-x}N$ barrier and AlN spacer layers, respectively. $d_T = d_{\mathrm{ox}} + d_{\mathrm{In_xAl_{1-x}N}} + d_{\mathrm{AlN}}$ is the total thickness, $V_{\mathrm{g0}} = V_{\mathrm{g}} - V_{\mathrm{off}} - V_{\mathrm{p}}$, V_{off} is the pinch-off voltage and V_{p} is the potential in the channel at in point p.

Substituting V_{g0} into Eq. 13, we obtain

$$n_s = \frac{\varepsilon(x)}{qd_T}\left(V_{\mathrm{g}} - V_{\mathrm{off}} - V_{\mathrm{p}} - E_{\mathrm{F}}\right). \tag{14}$$

The relationship of the quasi-Fermi level position and 2-DEG density n_s formed at the AlN/GaN heterointerface can be calculated using a relatively simple equation derived from the self-consistent solution of Schrodinger's and Poisson's equations in the triangular potential well is expressed as follows[18]

$$n_s = DV_T \sum_{i=0}^{1} \ln\left\{1 + \exp\left[\frac{E_{\mathrm{F}} - E_i}{V_T}\right]\right\}. \tag{15}$$

where $D = 4\pi.m^*/h^2$ is the conduction band density of states of a 2-DEG system in the triangular well system, m^* is the electron effective mass, h is the Planck's constant, $V_T = k_{\mathrm{B}}T/q$ is the thermal voltage, k_{B} is the Boltzmann's constant, T is the ambient temperature.

Now, by considering only the lowest subband first energy level term E_0, Eq. 15 becomes

$$n_s = DV_T \ln\left\{1 + \exp\left[\frac{E_{\mathrm{F}} - E_0}{V_T}\right]\right\}. \tag{16}$$

The Taylor's theorem approximation $\ln(1+x) \approx x$ for $x \ll 1$ is used in Eq. 16, it can be simplified as

$$\ln\left[\exp\left(\frac{E_{\mathrm{F}} - E_0}{V_T}\right) + 1\right] \approx \exp\left(\frac{E_{\mathrm{F}} - E_0}{V_T}\right). \tag{17}$$

Therefore, we have

$$\frac{n_s}{DV_T} = \exp\left(\frac{E_{\mathrm{F}} - E_0}{V_T}\right). \tag{18}$$

Equation 17 can be written as

$$V_T \ln\left(\frac{n_s}{DV_T}\right) = E_{\mathrm{F}} - E_0. \tag{19}$$

The aim of 2-DEG carrier density modeling is to develop explicitly the Fermi level E_{F} with respect to gate voltage V_{g0} expression as related to the precise solution as feasible, which is appropriate for drain current and other model development.

$$E_{\mathrm{F}} = E_0 + V_T \ln\left(\frac{n_s}{DV_T}\right). \tag{20}$$

Substituting for E_0 from the follow expression

$$E_0 = \gamma_0 n_s^{2/3}. \tag{21}$$

Equation 19 becomes

$$E_{\mathrm{F}} = \gamma_0 n_s^{2/3} + V_T \ln\left(\frac{n_s}{DV_T}\right), \tag{22}$$

$$E_{\mathrm{F}} = \gamma_0 n_s^{2/3} + V_T \ln(n_s) - \ln(DV_T), \tag{23}$$

where γ_0 is a constant estimated by Shubnikov De Hass or from cyclotron resonance experiments.

Next, assuming the gate depletion and channel depletion overlap to give a fully depleted ($In_xAl_{1-x}N$ layer is ionized completely), to eliminate n_s term, and we replace n_s into Eq. 23.

We have

$$E_{\mathrm{F}} = \gamma_0\left[\frac{\varepsilon(x)}{qd_T}\left(V_{\mathrm{g0}} - E_{\mathrm{F}}\right)\right]^{2/3} + V_T\left[\ln\frac{\varepsilon(x)}{qd_T}\left(V_{\mathrm{g0}} - E_{\mathrm{F}}\right)\right] - \ln(DV_T). \tag{24}$$

We are expanding on the right-hand side of the two terms to first order in the form of $(E_{\mathrm{F}}/V_{\mathrm{g0}})$. Then we can get

$$E_F = \gamma_0\left(\frac{\varepsilon(x)}{qd_T}\right)^{2/3}(V_{g0})^{2/3}\left(1-\frac{E_F}{V_{g0}}\right)^{2/3} + V_T\ln\frac{\varepsilon(x)V_{g0}}{qd_T} + V_T\ln\left(1-\frac{E_F}{V_{g0}}\right) - V_T\ln(DV_T), \tag{25}$$

Using Bernoulli's inequality approximation $(1+x)^n \approx 1+nx$ and the Taylor's theorem approximation $\ln(1+x)\approx x$ into Eq. 25, it can be simplified as

$$E_F = \gamma_0\left(\frac{\varepsilon(x)}{qd_T}V_{g0}\right)^{2/3}\left(1-\frac{2}{3}\frac{E_F}{V_{g0}}\right) + V_T\ln\frac{\varepsilon(x)V_{g0}}{qd_T} - V_T\frac{E_F}{V_{g0}} - V_T\ln(DV_T). \tag{26}$$

We can simplify Eq. 26 as

$$\frac{V_{g0}}{V_{g0}}E_F + \frac{2}{3}\gamma_0\left(\frac{\varepsilon(x)}{qd_T}V_{g0}\right)^{2/3} + V_T\frac{E_F}{V_{g0}} = \gamma_0\left(\frac{\varepsilon(x)}{qd_T}V_{g0}\right)^{2/3} + V_T\ln\frac{\varepsilon(x)V_{g0}}{qd_T} - V_T\ln(DV_T), \tag{27}$$

Thus, E_F can be expressed as

$$E_F = V_{g0}\frac{\gamma_0\left(\frac{\varepsilon(x)}{qd_T}V_{g0}\right)^{2/3} + V_T\ln\frac{\varepsilon(x)V_{g0}}{qd} - V_T\ln(DV_T)}{\frac{2}{3}\gamma_0\left(\frac{\varepsilon(x)}{qd_T}V_{g0}\right)^{2/3} + V_{g0} + V_T}. \tag{28}$$

At the site of 2-DEG accumulation, the total gate capacitance (C_g) is the *equivalent capacitance of three capacitors in* series-connected C_{ox},$C_{In_xAl_{1-x}N}$ and C_{AlN}, can be expressed as

$$\frac{1}{C_g} = \frac{1}{C_{ox}} + \frac{1}{C_{HEMT}}. \tag{29}$$

The capacitance of the barrier layer can be expressed as[19]

$$\frac{1}{C_{HEMT}} = \frac{1}{C_{In_xAl_{1-x}N}} + \frac{1}{C_{AlN}}. \tag{29a}$$

$$C_g = \frac{C_{ox}\times C_{In_xAl_{1-x}N}\times C_{AlN}}{C_{ox}\times C_{In_xAl_{1-x}N} + C_{ox}\times C_{AlN} + C_{In_xAl_{1-x}N}\times C_{AlN}}. \tag{29b}$$

where $C_{ox} = \varepsilon_0\varepsilon_{ox}/d_{ox}$ is the capacitance per unit area due to oxide layer and d_{ox} is the oxide layer thickness, $C_{In_xAl_{1-x}N} = \varepsilon_0\varepsilon_{In_xAl_{1-x}N}/d_{In_xAl_{1-x}N}$ represents the capacitance related to the barrier layer thickness $In_xAl_{1-x}N$ and $C_{AlN} = \varepsilon_0\varepsilon_{AlN}/d_{AlN}$ represents the capacitance related to the spacer layer thickness AlN.

Substituting for C_g into Eq. 28 gives

$$E_F = V_{g0}\frac{\gamma_0\left(\frac{C_gV_{g0}}{q}\right)^{2/3} + V_T\ln\left(\frac{C_gV_{g0}}{qDV_T}\right)}{\frac{2}{3}\gamma_0\left(\frac{C_gV_{g0}}{q}\right)^{2/3} + V_{g0} + V_T}, \tag{30}$$

Substituting Eqs. 29 and 30 into Eq. 13 we have

$$n_s = \frac{C_g}{q}(V_{g0}-E_F) = \frac{C_gV_{g0}}{q} - \frac{C_gE_F}{q}, \tag{31}$$

$$n_s = \frac{C_gV_{g0}}{q} - \frac{C_gV_{g0}}{q}\frac{\gamma_0\left(\frac{C_gV_{g0}}{q}\right)^{2/3} + V_T\ln(\delta V_{g0})}{\frac{2}{3}\gamma_0\left(\frac{C_gV_{g0}}{q}\right)^{2/3} + V_{g0} + V_T}, \tag{32}$$

where $\delta = \frac{C_g}{qDV_T}$.

$$n_s = \frac{C_gV_{g0}}{q}\frac{V_{g0} + V_T[1-\ln(\delta V_{g0})] - \frac{\gamma_0}{3}\left(\frac{C_gV_{g0}}{q}\right)^{2/3}}{\frac{2}{3}\gamma_0\left(\frac{C_gV_{g0}}{q}\right)^{2/3} + V_{g0} + V_T}. \tag{33}$$

Substituting $\theta = (\gamma_0/3)(C_g/q)^{2/3}$ the simplified expression for sheet charge density can be written as[20]

$$n_s = \frac{C_g}{q}\left[V_{g0}\frac{V_{g0}-\theta(V_{g0})^{2/3}}{V_{g0}+2\theta(V_{g0})^{2/3}}\right]. \tag{34}$$

I–V Characteristics Model for $Al_2O_3/In_xAl_{1-x}N$/AlN/GaN MOS-HEMTs

The expression for drain current through the channel using an analytical model is derived from Eq. 34, based on the 2-DEG sheet carrier density model that is developed in,[20] can be formulated as

$$I_{ds} = \frac{q\mu_0W_g}{L_g}\int_{V_s}^{V_d} n_s dV_p. \tag{35}$$

Where μ_0 is the low field mobility of the device, W_g is the gate width and L_g is the gate length.V_s and V_d are the source and drain voltages, respectively.

An analytical model of the drain current can be formulated as[9]

$$I_{ds} = \frac{\mu_0W_gC_g}{L_g\rho}\left[\sum_{i=1}^{6}k_i\left(\psi_{gd}^i - \psi_{gs}^i\right) + k_0\ln\frac{\psi_{gd}}{\psi_{gs}}\right]. \tag{36}$$

Where $\psi_{gs} = (V_{gs} - V_{th})^{1/3} + 2\theta$, $\psi_{gd} = (V_{gs} - V_{th} - V_{ds})^{1/3} + 2\theta$, $\rho = 1 - [(V_{ds} - V_s)/E_T L_g]$, E_T is the critical field, with a limit $V(p=0) = V_s = 0\,V$ and $V(p = L_g) = V_d = V_{ds}$. Table I gives the expressions for the constants $k_i (i = 1, \ldots, 6)$ obtained during the integration of Eq. 34.

Transconductance Model for $Al_2O_3/In_xAl_{1-x}N/AlN/GaN$ MOS-HEMTs

The transconductance is an important parameter extremely important for estimating the microwave performance of the device. In strong inversion, the transconductance is the major part of the power gain mechanism, it can be defined as

$$g_m = \left.\frac{\partial I_{ds}}{\partial V_{gs}}\right|_{V_{ds}=\text{const}}. \tag{37}$$

The transconductance can be extracted from Eq. 36[9]

$$g_m = -\frac{\mu_0 W_g C_g}{L_g \rho}\left[\frac{1}{3(\psi_{gd} - 2\theta)^2 - 3(\psi_{gs} - 2\theta)^2}\Omega_1\right]. \tag{38}$$

Where

$$\Omega_1 = \left[\begin{array}{l} \frac{288\theta^6}{(\psi_{gd}-\psi_{gs})} + 272\theta^5 + 1920\theta^4(\psi_{gd} - \psi_{gs}) + 600\theta^3(\psi_{gd} - \psi_{gs})^2 \\ -280\theta^2(\psi_{gd} - \psi_{gs})^3 + 195\theta(\psi_{gd} - \psi_{gs})^4 - 18(\psi_{gd} - \psi_{gs})^5 \end{array}\right]. \tag{38a}$$

Capacitances Model for $Al_2O_3/In_xAl_{1-x}N/AlN/GaN$ MOS-HEMTs

The gate capacitances C_{gs} and C_{gd} are derived from the partial differentiation of the total gate charges w.r.t $V_s = V_{gs}$ and $V_d = V_{ds}$ source and drain terminal voltages, respectively, and can be expressed as $C_{gs} = \partial Q_g/\partial V_{gs}$ and $C_{gd} = \partial Q_g/\partial V_{ds}$.[9]

The gate-to-source capacitance is obtained as[9]

$$C_{gs} = \frac{\mu_0 (qW_g\rho)^2}{I_{ds}}\left(\psi_{gd}^{1/3} - \psi_{gs}^{1/3}\right)\left(\frac{g_m}{I_{ds}} - 1\right) - \frac{qW\rho}{E_T}V_{ds} - \frac{L_g g_m}{\mu_0 E_T}. \tag{39}$$

The gate-to-drain capacitance is obtained as[9]

$$C_{gd} = \frac{\mu_0 (qW_g\rho)^2}{I_{ds}}\left(\psi_{gd}^{1/3} - \psi_{gs}^{1/3}\right)\left(\frac{g_d}{I_{ds}} - 1\right) - \frac{qW\rho}{E_T}\psi_{gd} - \frac{L_g g_d}{\mu_0 E_T}. \tag{40}$$

Unity Gain Cut-Off Frequency Model for $Al_2O_3/In_xAl_{1-x}N/AlN/GaN$ MOS-HEMTs

The unity gain cut-off frequency (f_T) can be obtained as[9]

$$f_T = \frac{g_m}{2\pi(C_{gs} + C_{gd})}. \tag{41}$$

All the data model parameters used in our calculations are listed in Table II.

RESULTS AND DISCUSSION

In this section, we have discussed the static and dynamic characteristics of GaN-based MOS-HEMTs with different indium mole fractions of (12, 15, 17, and 18)%, and the results are compared with experimental data taken from Ref. 22. The model parameters of $Al_2O_3/In_xAl_{1-x}N/AlN/GaN$ MOS-HEMTs device used for the calculation of the static and dynamic characteristics, for each of the two different device types are indicated in Table III.

Figure 3 shows the threshold voltage variations with indium mole fraction variations at different barrier layer thicknesses. It is observed that the

Table I. Constants terms obtained during the integration

Constant	Expression
k_0	$-288\theta^6$
k_1	$272\theta^5$
k_2	$-960\theta^4$
k_3	$200\theta^3$
k_4	$-70\theta^2$
k_5	39θ
k_6	-3

Table II. List of model parameters

Parameter	Value	Unit	References
E_T	178×10^5	V/m	9
ε_0	8.854×10^{-12}	F/m	15
ε_{InN}	$15.3\varepsilon_0$	F/m	15
ε_{AlN}	$10\varepsilon_0$	F/m	15
ε_{ox}	$10\varepsilon_0$	F/m	9
$\sigma_{ox/In_xAl_{1-x}N}$	-1.8×10^{17}	m^{-2}	21
$\sigma_{AlN/GaN}$	6.5×10^{17}	m^{-2}	21
$\Delta E_C^{ox/In_xAl_{1-x}N}$	1.8	eV	9
$\Delta E_C^{AlN/GaN}$	1.7	eV	16
Q_f	$+5 \times 10^{17}$	C/m^2	9
μ_0	0.06	m^2/Vs	9
γ_0	4×10^{-12}	–	10

Table III. Parameters and device details used for calculation

Parameter	Quantity	Sample 1	Sample 2[22]
V_{off} (V)	Pinch-off voltage	− 3.8[22]	− 3.8
d_{ox} (nm)	Oxide thickness	5[9]	3
$d_{In_xAl_{1-x}N}$ (nm)	Barrier thickness	13[1]	12
d_{AlN} (nm)	Spacer thickness	1[1]	1
L_g (μm))	Gate length	0.6[10]	0.6
W_g (μm)	Gate width	100[10]	100

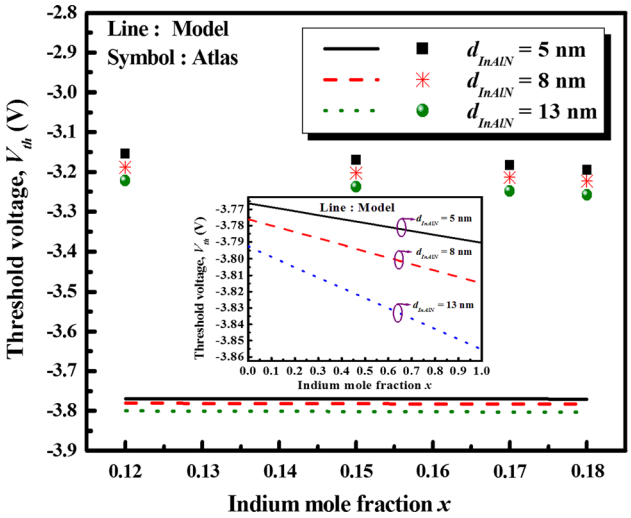

Fig. 3. Comparison of the threshold voltage of MOS-HEMTs modeled with MATLAB program and Atlas-TCAD simulation.

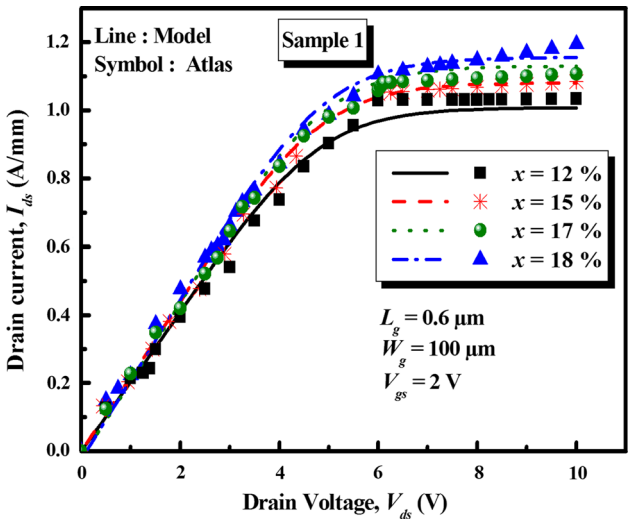

Fig. 4. Comparison of the output current characteristics of MOS-HEMTs modeled with different mole fractions.

threshold voltage reduces considerably in a linear manner with increasing indium mole fraction. As seen from this Fig. 3, V_{th} is lower for higher strain.

Figure 4 plots the output characteristics modeled with Atlas-TCAD simulation of $Al_2O_3/In_xAl_{1-x}N$/AlN/GaN MOS-HEMTs with different indium mole fractions x at V_{ds} = 2 V. The results show that for x = 18% the device reaches the maximum drain-to-source saturation current I_{dssat} = 1150 A/m compared with those obtained with x = (12, 15 and 17)%. Also, our results indicate that an improvement of the performance of MOS-HEMTs can be reached by varying the indium mole fraction in the $In_xAl_{1-x}N$ barrier layer. It is clear that our model results are in a good agreement with the one obtained by Atlas-TCAD data.

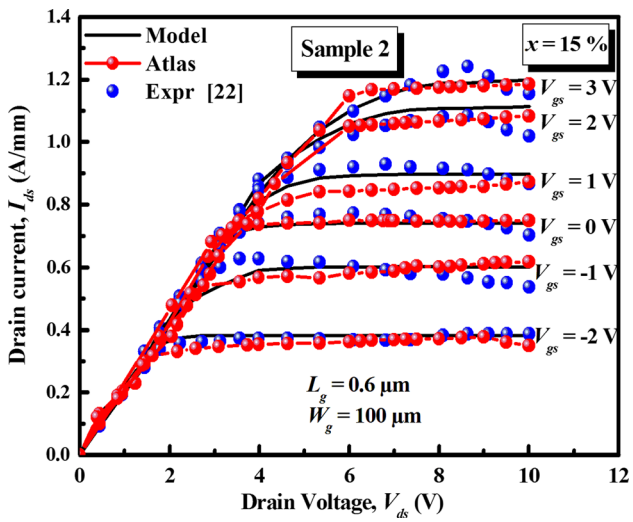

Fig. 5. Output current characteristics of MOS-HEMTs. Experimental data taken from Ref. 22.

Similarly, to validate the proposed model, exactly the same dimensions of $Al_2O_3/In_{0.15}Al_{0.85}N$/AlN/GaN MOS-HEMTs are considered for Atlas-TCAD and experimental data,[22] the device simulation as well as MATLAB calculations. The data sets from the device simulation serve as the input to the MATLAB program. Numerical calculations and solutions are performed by the MATLAB program and device simulation is done by Atlas-TCAD. Figure 5 shows comparison of the $I_{ds}(V_{ds})$ output characteristics modeled with MATLAB program, Atlas-TCAD simulation and experimental data[22] of the proposed $Al_2O_3/In_xAl_{1-x}N$/AlN/GaN MOS-HEMTs at indium mole fraction of x = 15%. The gate voltage varies from (− 2 to + 3) V with steps of + 1 V. The maximum drain current density of the

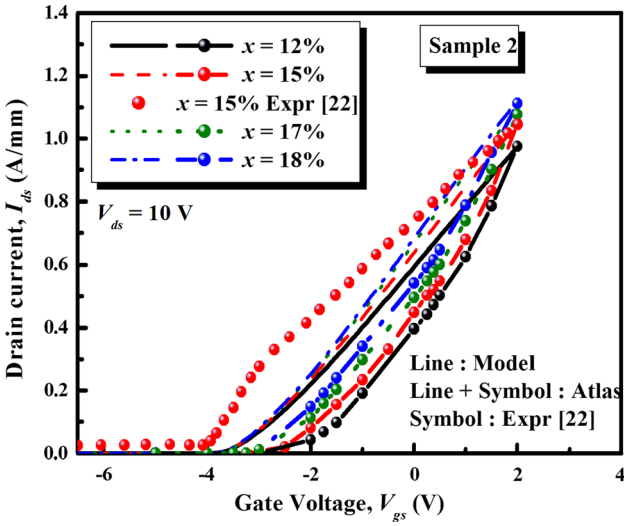

Fig. 6. Comparison of the $I_{ds}(V_{gs})$ transfer characteristics of MOS-HEMTs modeled with MATLAB program, Atlas-TCAD simulation with different mole fractions and experimental data taken from Ref. 22.

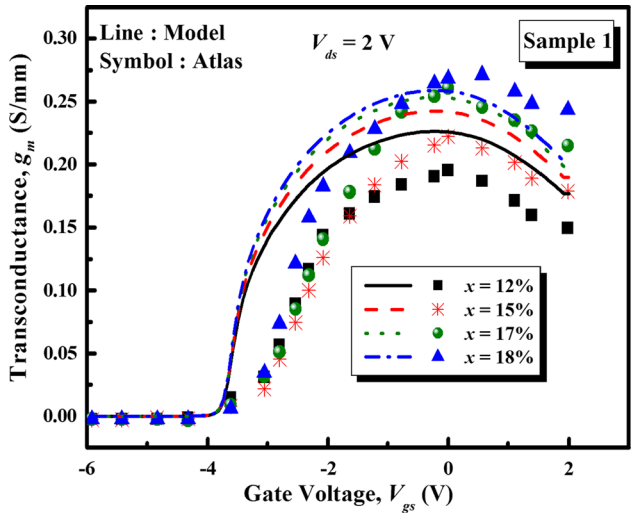

Fig. 7. Variation of the transconductance with gate-to-source voltage modeled with different indium mole fractions, MATLAB program and Atlas-TCAD.

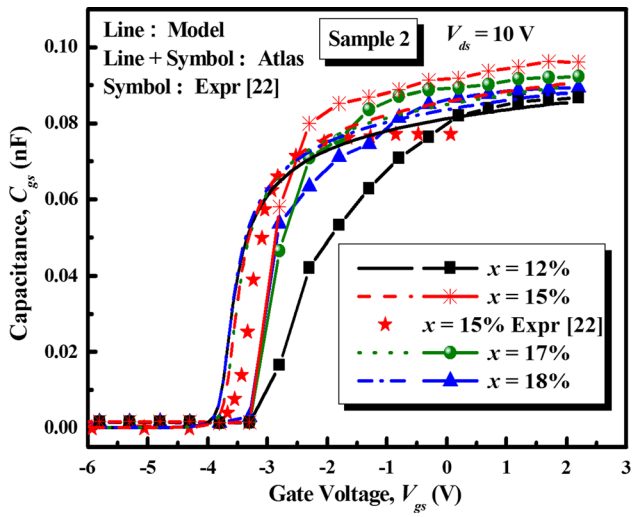

Fig. 8. Comparison of the gate-to-source capacitance modeled with MATLAB program, Atlas-TCAD simulation and experimental data taken from Ref. 22.

device at V_{gs} of 3 V is 1227 A/m. The *simulation* results show good agreement with the *experimental data, after the calibration.*

The $I_{ds}(V_{gs})$ transfer characteristics of the proposed GaN-based MOS-HEMTs modeled and simulated with different indium mole fractions are shown in Fig. 6. The validation of our results compared to the experimental data taken from Ref. 22 with x = 15%. Drain current increases with rising mole faction and very high drain current density. Also, it is clear that the results of our model of the transfer characteristics are in a good agreement with the one obtained by Atlas-TCAD data. The pinch-off voltage of −3.8 V of the modeled device shows exhibiting high drain current density of 1227 A/m at the same gate bias of 3 V with x = 15% indium mole fraction.

The combination of higher breakdown voltage and higher drain current implies that the proposed device is very much suitable for high power applications. Figure 7 shows the variation of the transconductance with V_{gs} varying from (− 6 to 2)V modeled with different indium mole fractions at $V_{gs} = 2$ V and a maximum transconductance rising of 268 S/m at $V_{gs} = 0$ V and indium mole fraction of 18% showing good agreement with our developed model and the simulation data.

The modeled results of the C–V characteristics have been carried out and compared with data obtained from Atlas-TCAD and experimental data. Figure 8 plots the variation of C_{gs} in terms of the gate voltage with drain voltage of 10 V. Our results show the dependence of threshold voltage on the indium mole fraction. The capacitance C_{gs} is small when V_{gs} is below or close to V_{off} and when V_{gs} increases C_{gs} rises. It is clear that the simulated model, the capacitance C_{gs} values obtained from Atlas-TCAD and the data taken from the experimental (concerning the 15% mole fraction value) agrees quite well.

Figure 9 shows a plot of gate-to-drain capacitance versus drain voltage of $Al_2O_3/In_xAl_{1-x}N/AlN/GaN$ MOS-HEMTs with MATLAB program and Atlas-TCAD simulation, with different indium mole fractions x at V_{ds} = 2 V. It is observed here that the capacitance is varying gradually with increase in drain voltage, when the device becomes saturated, so that the drain voltage can affect the charge in channel. A good correlation between the analytical model and Atlas-TCAD simulation result shows that the developed model is consistent with different mole fractions, which validates the capacitance modeling.

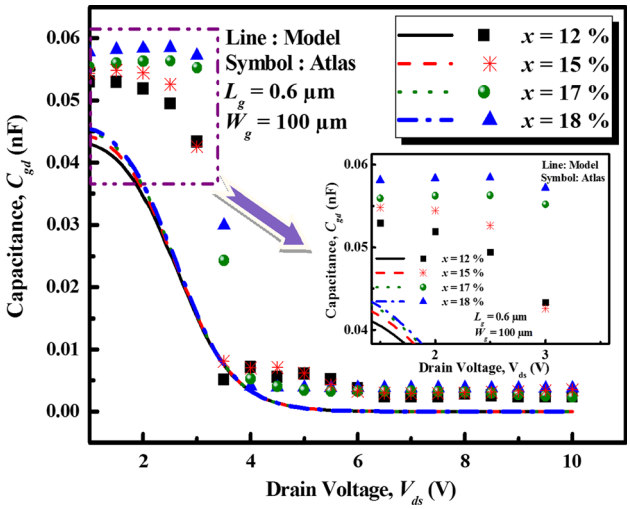

Fig. 9. Comparison of the gate-to-drain capacitance modeled with MATLAB program and Atlas-TCAD simulation.

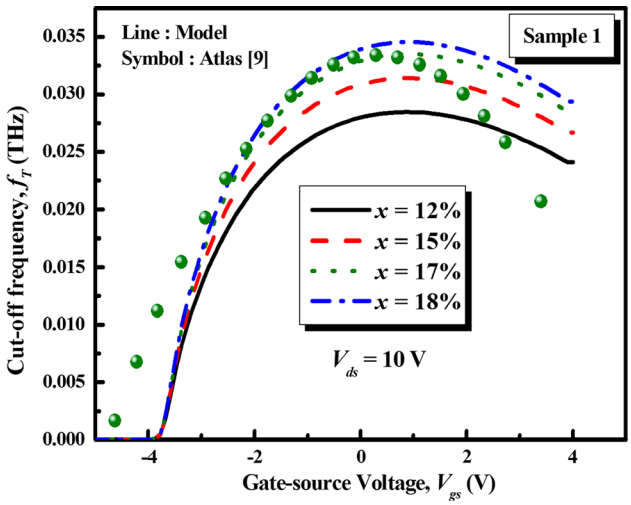

Fig. 10. Variation of the current gain cut-off frequency (f_T) with gate voltage modeled with MATLAB program results with different indium mole fractions and compared with Atlas-TCAD at indium mole fraction x = 17%.[9]

The influence of variation of the indium mole fraction (x) on the cut-off frequency (f_T) is shown in Fig. 10. The value of the cut-off frequency increases with the mole fraction as we can see in Fig. 10. This can be explained by the fact that the increase of the indium mole fraction leads to a higher electric field of induced polarization. As a result, the electron confinement in the channel increases. In Fig. 10 we notice a steady increase in the cut-off frequency as the gate bias increases from (− 4 to 0)V and then starts to decrease, once again we see that there is a good agreement between our analytical model calculations and the same results with Atlas-TCAD simulation data at indium mole fraction of x = 17% and V_{ds} = 10 V obtained by Jena et al.[9]

CONCLUSION

A physics-based fully analytical model for the static and dynamic characteristics of GaN-based MOS-HEMTs is proposed, analyzed and validated with Atlas-TCAD simulation results and experimental data. We have investigated the impact of the indium mole fraction on the drain current, the transconductance, the C-V characteristics, and the cut-off frequency. The proposed analytical models show excellent correlation with the Atlas-TCAD simulation and experimental data of GaN-based MOS-HEMTs, with different indium mole fractions, and it can be developed efficiently in radio frequency and microwave circuit designs. The parameters introduced in the model are clearly linked to physical effects and easily be extracted from experiments. The developed model will prove very useful in providing even more insight into the complete physics-based model for GaN-based MOS-HEMTs for performance analysis.

ACKNOWLEDGMENTS

The authors thank Benjamin Iñiguez from the Department of Electrical Electronics and Automation Engineering, University of Rovira i Virgili, Spain, for very valuable discussions and for careful reading of the manuscript.

REFERENCES

1. M. Gonschorek, J.F. Carlin, E. Feltin, M.A. Py, and N. Grandjean, *J. Appl. Phys.* 109, 063720 (2011).
2. M. Higashiwaki, T. Mimura, and T. Matsui, *Jpn. J. Appl. Phys. Part 2* 45, L1111 (2006).
3. J. Kuzmik, *IEEE Electron Device Lett.* 22, 510 (2001).
4. S. Lin, M. Eron, and A.E. Fathy, *IET Circuits Devices Syst.* 3, 135 (2009).
5. E. Sakalauskas, H. Behmenburg, C. Hums, P. Schley, G. Rossbach, C. Giesen, M. Heuken, H. Kalisch, R. Jansen, H. Bläsing, J. Dadgar, A. Krost, and R. Goldhahn, *J. Phys. D Appl. Phys.* 43, 5102 (2010).
6. R. Wang, P. Sanier, X. Xing, C. Lian, X. Gao, S. Guo, G. Snider, P. Fay, D. Jena, and H. Xing, *IEEE Electron Device Lett.* 31, 1383 (2010).
7. T.-C. Han, H.-D. Zhao, L. Yang, and Y. Wang, *Chin. Phys. B* 26, 107301 (2017).
8. O. Ambacher, B. Foutz, J. Smart, J.R. Shealy, N.G. Weimann, K. Chu, M. Murphy, A.J. Sierakowski, W.J. Schaff, and L.F. Eastman, *J. Appl. Phys.* 87, 334 (2000).
9. K. Jena, R. Swain, and T.R. Lenka, *IET Circuits Devices Syst.* 10, 423 (2016).
10. K. Jena, R. Swain, and T.R. Lenka, *Pramana—J. Phys.* 85, 1221 (2015).
11. *User Guide Manual*, ATLAS, Version 5.12.0.R./USA, Silvaco Inc (2010).
12. J. Kuzmik, *Semicond. Sci. Technol.* 17, 540 (2002).
13. V. Fiorentini, F. Bernardini, and O. Ambacher, *Appl. Phys. Lett.* 80, 1204 (2002).
14. F. Bernardini, in *Nitride Semiconductor Devices: Principles and Simulation*, ed. J. Piprek (Weinheim: Wiley-VCH, 2007), pp. 49–67.
15. Y. Zhou, Z. Lin, C. Luan, J. Zhao, Q. Yang, M. Yang, Y. Wang, Z. Feng, and Y. Lv, *Semicond. Sci. Technol.* 29, 095011 (2014).
16. M. Gonschorek, J.-F. Carlin, E. Feltin, M.A. Py, and N. Grandjean, *Int. J. Microw. Wirel. Technol.* 2, 13 (2010).
17. E. Iliopoulos, A. Adikimenakis, C. Giesen, M. Heuken, and A. Georgakilas, *Appl. Phys. Lett.* 92, 191907 (2008).

18. T.J. Drummond, H. Morkoc, K. Lee, and M. Shur, *IEEE Electron Device Lett.* 3, 338 (1982).
19. M. Lachab, M. Sultana, Q. Fareed, F. Husna, V. Adivarahan, and A. Khan, *J. Phys. D Appl. Phys.* 47, 135108 (2014).
20. M.F. Yigletu, S. Khandelwal, T.A. Fjeldly, and B. Iñiguez, *IEEE Trans. Electron Devices* 60, 3746 (2013).
21. G. Amarnath, R. Swain, and T.R. Lenka, *Int. J. Numer. Model. Electron. Netw. Devices Fields* 31, 1 (2017).
22. M. Wei, Z. Jin-Cheng, X. Jun-Shuai, H. Yao, M. Xiao-Hua, C. Wang, L. Hong-Xia, X. Sheng-Rui, Y. Lin-An, B. Zhi-Wei, L. Xiao-Zhen, Z. Jin-Feng, and K. Xian-Wei, *Chin. Phys. Lett.* 27, 128501 (2010).